


Collisionless Heating Driven by Vlasov Filamentation in a Counterstreaming Beams Configuration

Alain Ghizzo^{✉*} and Daniele Del Sarto[†]

Institut Jean Lamour, UMR 7198, Université de Lorraine, BP 70239 54506 Vandoeuvre les Nancy cedex, France

Homam Betar[‡]

Mécanique et Modélisation, Procédés Propres, UMR 7340 CNRS, Université de Aix-Marseille, 38 rue Joliot-Curie, 13451 Marseille, France

 (Received 15 March 2023; revised 10 May 2023; accepted 20 June 2023; published 18 July 2023)

We perform high resolution kinetic simulations of interpenetrating plasma beams. This configuration is unstable to both Weibel-type and two-stream instabilities, which are known to linearly induce a growth of the magnetic and electrostatic energy, respectively, at the expenses of the kinetic energy. “Oblique modes” are further beam-plasma instabilities, which linearly combine the features of the former two. Here we show the possibility of a reversal of the energy flow associated to these beam-plasma instabilities, when secondary propagating oblique modes are excited. This rapid conversion from magnetic to kinetic energy (i.e., kinetic heating), differs from the standard magnetic reconnection scenario and is induced by the reinforcement of the filamentation process of the distribution function in the phase space. This phenomenon—likely of general interest to collisionless dissipation processes in plasmas—can be understood in terms of mode synchronization: the coupling of oblique modes at disparate spatial scales leads to the appearance of synchronized “filamented” modes, which act on the global dynamics of the plasma via kinetic heating, collisionless dissipation, and turbulence.

DOI: [10.1103/PhysRevLett.131.035101](https://doi.org/10.1103/PhysRevLett.131.035101)

In a configuration characterized by two counterpropagating electron beams, which can be met in astrophysics [1], in laboratory astrophysics [2,3], and in laser-plasma accelerators [4], Weibel-type instabilities can couple with electrostatic unstable modes by generating the so-called oblique instabilities (OIs). In Ref. [5] a propagative branch of OI modes has been identified. Here we discuss and show via kinetic simulations—performed with both semi-Lagrangian [6] and particle-in-cell (PIC) Vlasov-Maxwell [7] codes—how the spatial filamentation induced by these modes is capable of affecting, both linearly and nonlinearly, the phase-space filamentation of the distribution function by synchronizing the phases of the Van Kampen modes [8]. This leads to large amplitude fluctuations of the distribution function in the phase space, to which hereafter we refer to as to an “enhanced filamentation.” This process occurs in combination with large amplitude, essentially reversible fluctuations of the entropy of the plasma (already shown in Ref. [9] to correspond to the violation of Casimir’s conservation in the Vlasov system) and is characterized by a change in the saturation regime of the OIs, where the energy stored in the magnetic field can be transferred back to plasma particles via a kinetic heating mechanism. Note that phase-space filamentation is an intrinsic property of the Vlasov equation and does not refer, here, to the *spatial* filamentation of the “current filamentation instability” (CFI) [10]—although, after integration over the velocity

coordinate, phase-space filamentation becomes generally manifest at a macroscopic, fluid-scale description, as a filamentation in the coordinate space. Demonstrating this enhanced filamentation process is difficult, especially in the developed turbulence regime, due to its possible coupling with magnetic reconnection (MR). However, the counterpropagating beam configuration we start from provides an ideal framework for this analysis: in the 2D-2V geometry we consider here (which does imply appreciable results from the 2D-3V case [9]), it excludes the possibility of MR to occur, even as a secondary processes to the beam-plasma instabilities, which we will show instead to allow the amplification of the phase-space filamentation of f to a sufficiently high level to permit a reversal of the energy transfer.

Introduction.—The well-known filamentation phenomenon of f in the velocity space reflects an intrinsic property of the Vlasov equation. It is induced by the advection term (free streaming term) in the configuration space (see, e.g., [11], Sec. 5.4), and its “reversible” nature becomes manifest through the phenomenon of plasma echoes (see, e.g., [12], Sec. 4.2). Phase space synchronization of oscillators [13] is a key ingredient of phase mixing, which is at the basis of the collisionless Landau damping. This concept was used to study wave-particle interactions in the Vlasov-Poisson system [14,15] and in the gyrokinetic formalism [16,17]. Filamentation combined with synchronization can

violate another feature of the reversible, conservative VM system: the conservation of Casimir invariants. This can be indeed shown to follow from Liouville's theorem and Vlasov transport equation, only provided the distribution function f be sufficiently "smooth" at any time. In that case, the phase-space fluctuations of f , induced by filamentation, are not too large [18–20] and the solution of Vlasov equation is then weakly convergent in the sense of distributions.

The initial counterstreaming electron beam configuration is unstable to a number of modes: the transverse Weibel-type modes, either driven by pressure anisotropy of each beam (pure Weibel mode) [21] or, when the wave vector \mathbf{k} is perpendicular to the beams direction, by momentum anisotropy (transverse CFI) [22]; the longitudinal, electrostatic, two-stream instability, when \mathbf{k} is parallel to the beams; the *oblique instabilities* (OIs) when \mathbf{k} forms an angle different from $\pi/2$ with the beams [23–25]. Two branches of OIs, have been identified for propagation angles comparable to $\pm\pi/4$ with respect to the beams [5] (cf. Appendix A): a weakly propagative (dominant) branch with $\text{Re}(\omega) \lesssim 0.1\omega_{pe}$, to which from now on we will refer to as "nonpropagative" or as branch "A," and a higher frequency branch with $\text{Re}(\omega) \gtrsim 0.5\omega_{pe}$, which from now on we will refer to as "propagative" or to as branch "B," but which typically displays smaller growth rates than the nonpropagative modes. In Ref. [9] it was shown that the simultaneous excitation of several OI-B modes nonlinearly induces an excitation of high-frequency number OIs: this occurs as a direct turbulent-like cascade associated to a filamentation process of the distribution function in the coordinate space, and then in the phase space. Below we discuss how this process is related to a reversal of the transfer from the magnetic to the kinetic energy component associated to the growth of the initial OI: the corresponding kinetic heating is made possible by a synchronization process occurring during the linear stage of the secondary OI-B.

Physical model.—We consider a collisionless VM plasma, in the limit in which ions constitute a fixed uniform neutralizing background of density n_0 . Two counterpropagating electron beams (label $\alpha = 1, 2$) move along y with uniform initial velocities normalized to the light velocity $\beta_\alpha = u_{0,\alpha}/c$, in a two-dimensional geometry: $\mathbf{x} = (x, y, 0)$, $\mathbf{p} = (p_x, p_y, 0)$ are the relativistic particle position and momenta, so that $\gamma = \sqrt{1 + p^2/m^2c^2}$ is the Lorentz factor, m and $-e$ being the electron rest mass and charge. The electromagnetic (e.m.) fields read $\mathbf{E} = (E_x, E_y, 0)$ and $\mathbf{B} = (0, 0, B_z)$. Current neutralization $\sum_\alpha n_\alpha \beta_\alpha = 0$ is initially assumed. For the sake of simplicity we restrict our analysis to symmetric counterpropagating beams ($\beta_1 = -\beta_2$) having the same normalized thermal velocities $\sqrt{k_B T/mc^2}$ both along x and y : at perpendicular propagation this rules out the coupling between electrostatic and

e.m. modes [26]. The Vlasov equation is invariant under time reversal and inherits the conservation laws of Hamiltonian dynamics, e.g., that of the energy [i.e., the kinetic energy of particles, $\epsilon_K = (1/V) \int d^3x \int d^3p mc^2 \gamma f$ plus that of fields, $\epsilon_m = (1/2V) \epsilon_0 \int d^3x (E^2 + c^2 B^2)$], which we write as $\epsilon = \epsilon_K + \epsilon_m$, and the conservation of any "Casimir's invariant," i.e., of functionals $\int d^3x d^3p \mathcal{F}[f(\mathbf{x}, \mathbf{p}, t)]$ defined for arbitrary (yet sufficiently regular [18–20]) functions \mathcal{F} of f (see Ref. [27] for complements). Notice that the restriction to a 2D-2V geometry with $\partial/\partial z = 0$, combined with the initial configuration, at most compatible with a magnetic field $B_z(x, y, t)$, excludes the occurrence of MR.

Phase synchronization.—By writing the Vlasov equation in Fourier space as

$$\partial_t f_k(\mathbf{p}, t) = -i\mathbf{k} \cdot \mathbf{p} f_k / (m\gamma) + R_k(\mathbf{p}, t), \quad (1)$$

where $R_k(\mathbf{p}, t) = |R_k| e^{i\Theta_k(\mathbf{p}, t)}$ is the Fourier transform of the quantity $R(\mathbf{x}, \mathbf{p}, t) = -e[\mathbf{E} + \mathbf{p} \times \mathbf{B} / (m\gamma)] \cdot \nabla_p f$, we recognize in the $-\mathbf{k} \cdot \mathbf{p} f_k / (m\gamma)$ convection term the source of filamentation: strong spatial gradients (i.e., large values of $|\mathbf{k}|$) lead to stress forces related to the fluid strain, which cause a local enhancement of the collisionless "dissipation" via phase mixing. The coupling of filamentation with forces can indeed lead to collisionless heating [43–45] or to an irreversible dissipation via coarse graining. We recall that the latter consists in the sampling of a formally continuum domain with "unit cells," in which fine details are smoothed out according to some criterion. However, the fact that filamentation, by itself, is a "kinematic" process driven by the convection term in transport equation under the validity of Liouville's theorem is evident if one looks at the free streaming motion of a distribution of particles in absence of forces and of dissipation, namely, $\partial f / \partial t + v \partial f / \partial x = 0$ (cf. Fig. 3 later and Appendix B; see also Sec. 5.4 of Ref. [11]).

The phase $\varphi_k(\mathbf{p}, t)$ and amplitude $|f_k|$ of the distribution function $f_k(\mathbf{p}, t) = |f_k| e^{i\varphi_k}$ in Fourier space evolve according to

$$\partial_t |f_k| = |R_k| \cos(\Theta_k - \varphi_k), \quad (2)$$

$$\partial_t \varphi_k = -\mathbf{k} \cdot \mathbf{p} / (m\gamma) + (|R_k| / |f_k|) \sin(\Theta_k - \varphi_k). \quad (3)$$

Equations (2)–(3) can be read as an extension of Kuramoto's model [46,47] to a Hamiltonian system. Following Ref. [48], the Kuramoto model can be derived from the Hamiltonian $H = \sum_i J_i \omega_i + Kr \sum_i J_i \sin(\bar{\varphi} - \varphi_i)$, in the action-angle variables J_i, φ_i . Thus, Eq. (3) is similar to $\dot{\varphi}_i = \omega_i + Kr \sin(\bar{\varphi} - \varphi_i)$ of Kuramoto's model, describing the weak interaction of $i = 1, \dots, N$ oscillators of natural frequency ω_i and phase φ_i , $\bar{\varphi}$ being the average phase of the ensemble. K is the coupling parameter and r a real quantity ($0 \leq r \leq 1$), which measures the coherence of the

system. Equation (2) takes the form of $\dot{J}_i = -\partial H/\partial \varphi_i = KrJ_i \cos(\bar{\varphi} - \varphi_i)$, which indicates that $|f_k|$ plays the equivalent role of an action J_i . In the microcanonical description, it is possible to define, for each oscillator i , a “metric entropy” $S_i = k_B \ln J_i$; the metric entropy relies on a scheme for partitioning the phase space into elementary cells. For the Vlasov model, the entropy density is $S_k = -k_B \ln |f_k|$. This leads to the insight that the evolution towards phase synchronization is equivalent to the evolution towards a state of decreasing entropy, e.g., from a chaotic state to a synchronized state (see Refs. [48–50]). Conversely, the combination of filamentation and of coarse graining of f leads to an increase of the metric entropy. Thus, synchronization and filamentation are two antagonistic processes globally leading to the conservation of entropy if the level of fluctuations remains low.

Enhanced filamentation.—The phenomenon we are going to highlight via numerical simulations is related to the linear onset of OIs, so it is informative to study the behavior of f not far from the equilibrium configuration $f(\mathbf{x}, \mathbf{p}, 0) = \sum_j \frac{1}{2} F_{0j}(p_x, p_y + C_j) = F_0$, where F_{0j} is the Maxwellian distribution of the j th beam of canonical momentum C_j . Writing $f(\mathbf{x}, \mathbf{p}, t) = F_0(\mathbf{p}) + \delta f_k(\mathbf{p}, t)e^{ik \cdot \mathbf{x}} + \text{c.c.}$, (where c.c. denotes the complex conjugate), expressing the e.m. fields as $E_{xk} = |E_{xk}|e^{i\theta_x}$, $E_{yk} = |E_{yk}|e^{i\theta_y}$ and $B_{zk} = |B_{zk}|e^{i\theta_z}$, and separating the real and imaginary parts, the linearized Vlasov equation reads

$$\partial_t |\delta f_k| = -eF_0(\mathbf{p}) \sum_{j=x,y} p_j |E_{jk}| \cos(\theta_j - \varphi_k). \quad (4)$$

The evolution of the second order variation of the e.m. spectral energy density [apex “(2)”] $\epsilon_{m,k} \equiv \frac{1}{2} \epsilon_0 (|E_{xk}|^2 + |E_{yk}|^2 + c^2 |B_{zk}|^2)$ reads

$$\partial_t \epsilon_{m,k}^{(2)} = e \int d^2 p |\delta f_k| \sum_{j=x,y} \left(\frac{p_j}{m\gamma} |E_{kj}| \cos(\varphi_k - \theta_j) \right) \quad (5)$$

or, equivalently, $\partial_t \epsilon_{m,k}^{(2)} = -\delta \mathbf{E} \cdot \delta \mathbf{J}$. Using Vlasov equation this can be also expressed as

$$\partial_t (\epsilon_{m,k}^{(2)} + \epsilon_{\varphi,k}) = 0, \quad \epsilon_{\varphi,k} \equiv - \int d^2 p \frac{|\delta f_k|^2 p_x}{2 \frac{\partial F_0}{\partial p_x} m\gamma}, \quad (6)$$

which generalizes the “energy” relation obtained by Kruskal and Oberman [51,52] to the e.m. case, via the introduction of the “phasestrophy” flux density $\epsilon_{\varphi,k}$. The phasestrophy $S_\varphi = \int (d^3 x/V) \int d^3 p \delta f^2 / [2 \partial F_0 / \partial p_x]$ introduced in Ref. [53] in the context of gyrokinetic tokamak turbulence is not a formal Casimir but it is a sort of an L^2 norm representing the phase space density auto-correlation function linked to the growth of filaments. Equation (6), obtained using the real part of the Fourier decomposition

related to Eqs. (2)–(3), highlights an energy transfer, occurring during the linear stage of an instability, which takes place in combination with the conservation (non-linearly valid) of the total energy e . The variation of $\epsilon_{\varphi,k}$ during an OI can be interpreted (similarly to what was earlier shown in tokamak turbulence [53]) in terms of a momentum transfer [54], of which we take here $\epsilon_{\varphi,k}$ as a proxy in numerical simulations (cf. also Appendix B). The physical mechanism behind (6) can be understood in terms of phase synchronization, by considering the imaginary part of the Fourier representation associated with the Kuramoto-type model, and by introducing the quantity $\epsilon_{m,k}^{(2)} \equiv \frac{1}{2} (|E_{xk}|^2 + |E_{yk}|^2 - c^2 |B_{zk}|^2)$:

$$\epsilon_{m,k}^{(2)} \frac{\partial \Theta_k}{\partial t} = - \int d^2 p \frac{p_x}{2m\gamma} \frac{|\delta f_k|^2}{\frac{\partial F_0}{\partial p_x}} \left(\frac{\partial \varphi_k}{\partial t} + \frac{\mathbf{k} \cdot \mathbf{p}}{m\gamma} \right). \quad (7)$$

For OIs, $\partial \Theta_k / \partial t$ is close to the mode frequency. For OI-A modes $\partial \Theta_k / \partial t \simeq \omega_A \simeq 0$, but for OI-B modes $\partial \Theta_k / \partial t \simeq \omega_B \neq 0$. One can also expect that nonlinearly $\partial \varphi_k / \partial t + \mathbf{k} \cdot \mathbf{p} / (m\gamma) \simeq 0$ because of small-scale filamentation. As we are going to show via numerical results, this also happens in the linear and early nonlinear stage of secondary OI-B modes because of a synchronization process induced by the OI-B-driven spatial filamentation. This phase locking, together with the divergence of the phasestrophy density, makes the left-hand side term of (7) finite for OI-B modes. In the linear stage of OI-B modes, the increase of $\epsilon_{\varphi,k}$, related to the acceleration of particles corresponding to the dynamical enhancement of a phase-space filament, induces a decrease of the e.m. energy density because of the constraint $\epsilon_{m,k}^{(2)} + \epsilon_{\varphi,k} = \text{cste}$.

Numerical experiments.—The process described in previous section has been identified via simulations performed with equivalent parameters with two different numerical schemes, used because of their complementarity in dealing both with filamentation and synchronization (see Ref. [27]): the semi-Lagrangian code VLEM [6] and the PIC code SMILEI [7]. The “numerical experiments” discussed below differ because of the size $L_x \times L_y$ of the coordinate domain (be $V \equiv L_x L_y$ its volume), which allowed us to excite a different set of initial modes. The maximum growth rates found using the procedure described in [5] are for $(k_x c / \omega_{pe}, k_y c / \omega_{pe}) = (3.0, 5.0)$ for the OI-A mode and for (5.0, 2.0) for the OI-B mode. Simulations have been initialized with an initial Maxwellian equilibrium, for a beam configuration with $|\beta_{1,2}| \simeq 0.514$ and $T_1 = T_2 = 6$ keV. In all runs, the total energy is well preserved and displays a variation of $\sim 0.1\%$ during the whole simulation. In the Supplemental Material [27] the numerical parameters are summarized and VLEM and SMILEI simulation results are compared. Figure 1 shows the results of two simulations performed with the VLEM code, noted A and B, initialized so to excite the

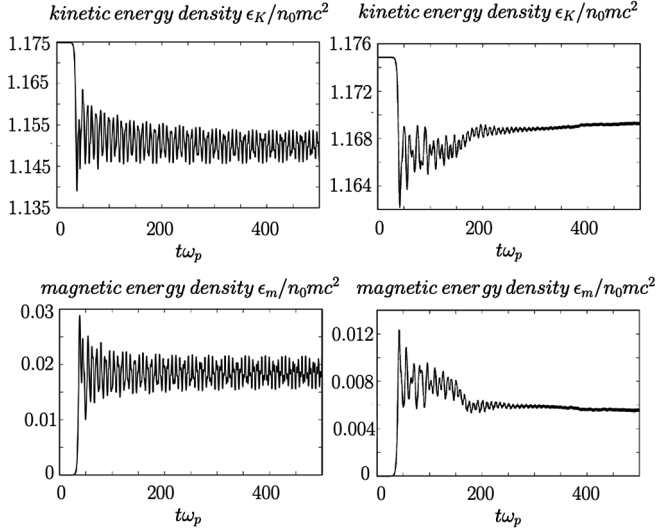


FIG. 1. On the left frames, on top, the kinetic energy ϵ_K versus time, on bottom, the magnetic energy ϵ_m versus time, for the nonpropagative OI-A mode (VLEM, case A). On the right frames, the corresponding ϵ_K (on top) and ϵ_m (on bottom) for the propagative OI-B mode (VLEM, case B). The contributions of the electric energy component ϵ_e are negligible.

OI-A mode only (left frames, case A) and to allow for a transition from the low-frequency OI-B to the high-frequency OI-B mode (right frames, case B), respectively. The excitation and linear growth of the OI-A mode takes place in the first stage followed by the expected nonlinear saturation: in the top left panel is shown the kinetic energy variation; the corresponding evolution of the magnetic energy $\epsilon_m \simeq (1/2\epsilon_0) \int (d^2x/V) B_z^2$ is shown in the bottom left panel. In the right column, in Fig. 1, the same diagnostics are shown for the propagative mode OI-B of the simulation case B. In the latter, the initial perturbation has been chosen so to excite small-frequency OI-B modes [5] in a region of the parameter space where nonlinear coupling can spontaneously lead to the excitation of the high-frequency OI-B [9]. Up to the time $t\omega_p \leq 150$, the dynamics of the OI instability is very similar to the previous case, except that the magnetic energy reaches a saturation level with twice the amplitude of case A. However, a secondary instability appears in the second phase of the evolution, when the energy transfer is reversed: the magnetic energy decreases and is converted into kinetic energy. In both simulations the electric energy remains negligible.

To analyze in detail the underlying physical mechanism we show in Fig. 2 the time evolution of the global phasestrophy flux $\epsilon_\varphi = -\int (d^2k/V) \epsilon_{\varphi,k}$ [cf. Eq. (6)]. Thanks to the absence of noise associated with the semi-Lagrangian scheme of the VLEM solver, ϵ_φ allows us to measure the rate of enhanced filamentation of f induced by the synchronization mechanism which appears in a dominant way in the saturation phase of the OI instability. An amplification of the total phasestrophy flux in the saturation

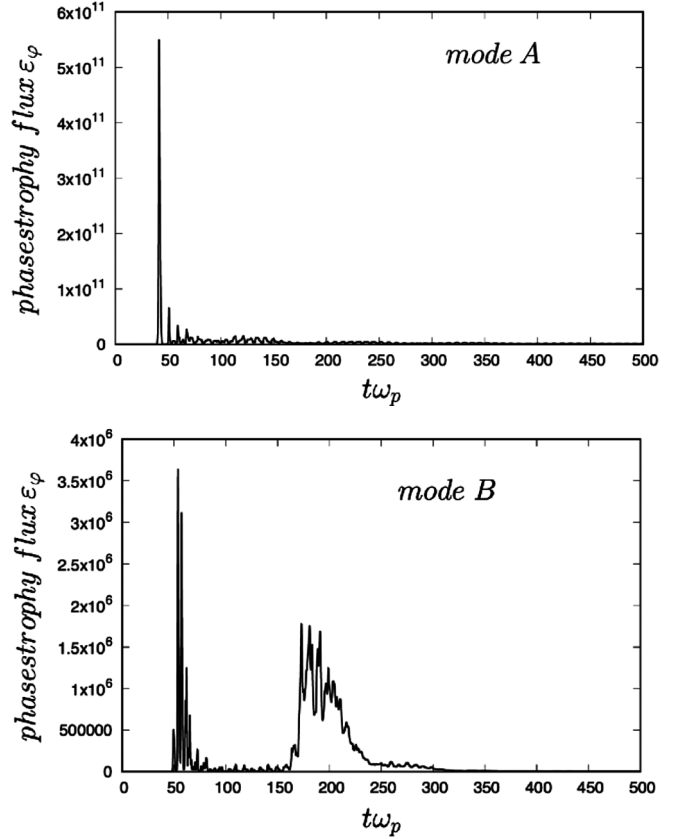


FIG. 2. Time history of the total phasestrophy flux of the OI-A mode (top frame, VLEM case A) and of the propagative OI-B mode (bottom frame, VLEM case B). The occurrence of a second peak in the bottom frame is associated with the energy conversion reversal.

phase of the primary instability is observed in both simulation cases A and B; however, in the case B, the second peak of ϵ_φ at $150 \leq t\omega_p \leq 200$ is a signature of the momentum transfer associated to a resurgence of the filamentation process during the conversion of the magnetic energy into kinetic energy (cf. Fig. 1, right frames). The enhanced filamentation appears in the phase-space as the generation of thin filaments at the center of a vortex structure. These are shown in the left frame of Fig. 3, for the nonlinear stage of a simulation case-B, this time performed with SMILEI (see also the corresponding animation in Ref. [27]). For comparison, the left frame of Fig. 3 shows “standard” kinematic phase-space filaments, generated by convection in an example of a free streaming distribution function, as discussed in Sec. 5.4 of Ref. [11].

A third simulation (case C—see Ref. [27]) highlights the connection between the enhanced filamentation and the violation of Casimir’s conservation, namely, the entropy $S = -k_B \int (d^2x/V) \int d^2p f \ln f = V \int d^2k \int d^2p S_k |f_k|$. To this purpose, a large spectrum ($0 \leq k_x, k_y \leq 20$) of both OI-A and OI-B modes has been linearly excited so as to induce a stronger heating mechanism. The evolution of this

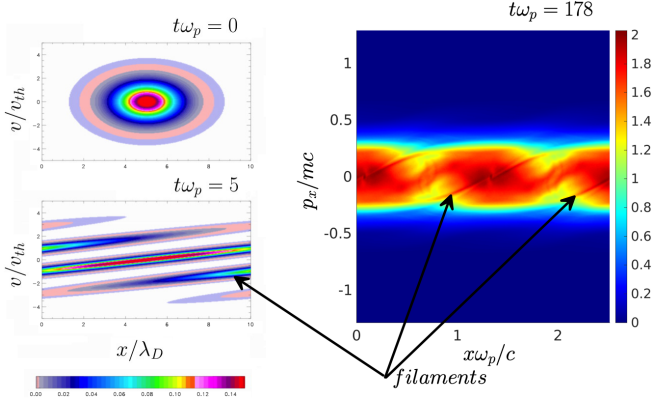


FIG. 3. Left: formation of phase-space filaments as an initial Gaussian distribution evolves according to $\partial_t f + v\partial f/\partial x = 0$ in the normalized phase-space $(x/\lambda_d, v/v_{th})$, where λ_d et v_{th} are the electron Debye length and thermal velocity, respectively (example and figure taken from §5.4 of Ref. [11]). Right: formation of filaments in the enhanced filamentation process, in the simulation case B performed with the SMILEI code. The time $t\omega_p \simeq 178$, corresponds to the second peak observed in the time evolution of the phasestrophy (cf. Fig. 2).

system displays a sort of (almost) “closed cycle” in the (S, ϵ_K) diagram, shown in the top frame of Fig. 4: the final and initial configuration states (respectively, shown in the (p_x, p_y) plane in the bottom frames of Fig. 4) differ but, as

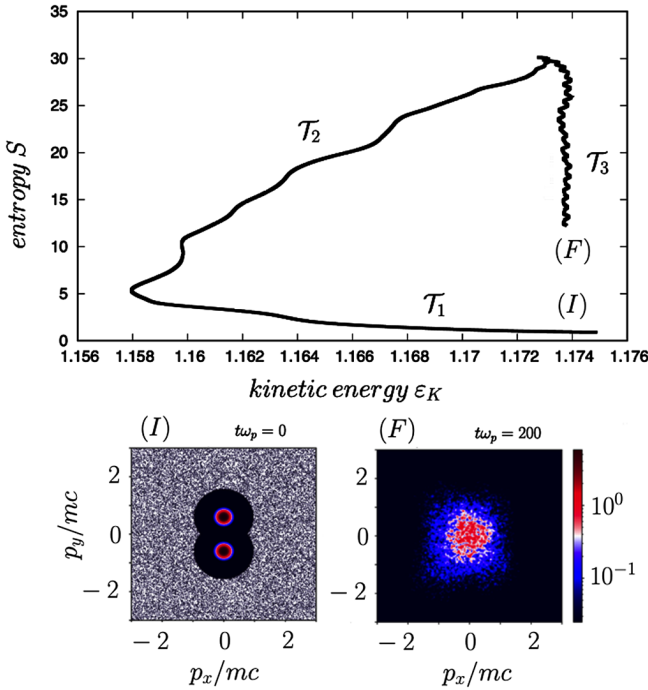


FIG. 4. Top frame: Almost reversible (cyclic) entropy variation in the entropy-kinetic energy plane (S, ϵ_K) in the simulation case C performed with VLEM: an adiabatic transformation (\mathcal{T}_1), a transformation due to the enhanced filamentation (\mathcal{T}_2) and a transformation with $\epsilon_K \simeq \text{const}$ (\mathcal{T}_3) can be recognized. Bottom frame: Phase-space patterns of the initial (left) and final state (right) in the (p_x, p_y) plane.

the kinetic energy ϵ_K evolves, S undergoes an almost globally reversible, macroscopic variation. This is allowed by the violation of the Casimir conservation induced by the enhanced filamentation process, and is composed of three thermodynamic transformations \mathcal{T}_1 - \mathcal{T}_3 (see also Appendix B). Although the detailed features of this “cycle” will be discussed elsewhere, its general features can be understood in terms of the enhanced filamentation scenario: \mathcal{T}_1 is quasiadiabatic, coherently with the Hamiltonian character of the Vlasov-Maxwell system; it corresponds to the linear growth of OIs, where the kinetic energy is converted into magnetic energy. \mathcal{T}_2 is related to the enhanced filamentation process and is characterized by the increase of both kinetic energy and entropy. \mathcal{T}_3 , “isothermal,” with $\epsilon_K \simeq \text{const}$, takes place in the strongly coupled Kuramoto system, which evolves from a high to a low entropy state because of the global synchronization.

Conclusions.—We have shown how an enhanced (phase-space) filamentation, here interpreted as due to a Kuramoto-type synchronization of undamped harmonic plasma oscillations (Van-Kampen modes [8]), can be identified by quantifying the “phasestrophy” of the system (cf. Refs. [53,54]). It leads to a kinetic heating occurring at the expenses of the magnetic energy. A reversal of the energy transfer from “kinetic \rightarrow magnetic” to “magnetic \rightarrow kinetic” had been already observed, when MR develops after an initial process of magnetic field amplification, although a different geometry than the one we considered is required to account for MR in the Weibel-unstable configuration we started from [55–59]. The “magnetic \rightarrow kinetic” energy conversion mechanism discussed here and related to the “enhanced” amplification of the kinematic filamentation process intrinsic to the Vlasov equation, appears therefore to be more general than MR itself. On the other hand, collisionless MR can originate from filamentation because of phase mixing (see, e.g., Refs. [60–65]) or of other “coarse-graining” mechanisms [66,67], which can be also modeled in terms of an anomalous resistivity due to the stochasticity of the turbulent magnetic fluctuations (see, e.g., Refs. [68–70]). This suggests the possible fundamental character of the kinetic heating process we have identified and calls for future dedicated investigations, aimed at shedding light into its role in both MR and in the turbulent energy cascade. Also the characterization, in terms of information theory (see, e.g., Refs. [54,65]), of the reversible or irreversible character of the entropy evolution in the transformations of simulation case C merits further studies (cf. Appendix B).

The results we have discussed here can be relevant to laser-plasma experiments (see Refs. [1,2,4]), to the electron heating mechanisms in relativistic shock waves (see Refs. [71,72]), as well as to *in situ* spacecraft measures of the solar-wind and magnetosphere turbulent interaction (see Refs. [73,74]).

The authors are grateful to the IDRIS computational centre, Orsay, France, for computer time allocation on their machines. This work was granted access to the HPC resources (Grant No. A0130507290) made by the “Grand Equipement National de Calcul Intensif” (GENCI) and has been partially funded by the French Federation for Magnetic Fusion Studies (FR-FCM) through the FR-FCM AAP-2021 “Evolution of current sheets in low-collision plasmas.” The views and opinions expressed herein do not necessarily reflect those of the European Commission. During the completion phase of this work, one of the authors (H. B.), formerly at IJL (Nancy), received financial support from the AIM4EP project (ANR-21-CE30-0018), funded by the French National Research Agency (ANR).

Appendix A: Oblique modes in the counter-streaming beam configuration.—We recall here some key features of the OI-A and OI-B modes identified in Refs. [5,9] and which are referenced in the main text. Linearization of the Vlasov-Maxwell system for an initial symmetric beam configuration and for a perturbation with $\mathbf{k} = (k_x, k_y, 0)$ (cf. physical model section) yields the dispersion relation

$$(\omega^2 \varepsilon_{xx} - k_y^2)(\omega^2 \varepsilon_{yy} - k_x^2) - (\omega^2 \varepsilon_{xy} + k_x k_y) = 0, \quad (\text{A1})$$

written in terms of the dielectric tensor elements

$$\varepsilon_{\alpha\beta} = \delta_{\alpha\beta} + \frac{\varepsilon_0 \omega_p^2}{\omega^2} \int \frac{p_\alpha \partial f_0}{\gamma \partial p_\beta} d^3 p + \frac{\varepsilon_0 \omega_p^2}{\omega^2} I, \quad (\text{A2})$$

where $\omega_p^2 = n_0 e^2 / m \varepsilon_0$ is the squared plasma frequency and $I = \int (p_\alpha p_\beta / \gamma) \{ [\mathbf{k} \cdot (\partial f_0 / \partial \mathbf{p})] / (m \gamma \omega - \mathbf{k} \cdot \mathbf{p}) \} d^3 p$. The initial counterstreaming electron beam distribution f_0 is chosen to be a double-Maxwellian, which describes two symmetric beams of equal, isotropic temperatures. The isotropic temperature condition rules out the coupling with pure Weibel modes, whereas the condition of symmetry of the beams, up to their second order fluid moments (i.e., density, velocity, and pressure) rules out the linear coupling with electrostatic modes [26]. As an example, Fig. 5 shows the normalized value $\Gamma(k_x, k_y) / \omega_{pe}$ of the imaginary part of some of the roots of Eq. (A1), evaluated for $p_2 \simeq 0.90 mc = -p_1$ and $T_1 = T_2 = 6$ keV: the growth rates of the TSI ($k_y = 0$) and of the CFI ($k_x = 0$), typically larger in absolute value than those of the OIs, are not represented in the contour plot, whereas the two branches corresponding to the OI-A and OI-B modes are explicitly indicated, therein. The OI-A mode (label A) corresponds to the upper lobe. The OI-B mode (label B), corresponding to the lower lobe, displays a significantly lower growth rate (and because of this it is typically neglected in the counting of the “roots” of the OI—see, e.g., Refs. [23–25]) but has a higher frequency. Determining the roots of the kinetic dispersion relation

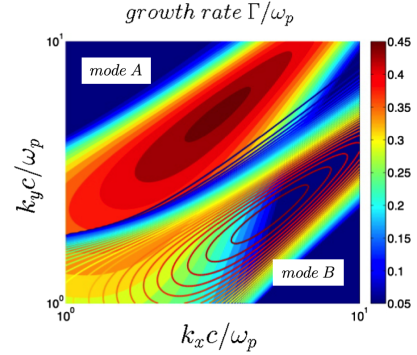


FIG. 5. Contour plot of the growth rate of the oblique “filamentation” instability in the normalized $(k_x c / \omega_{pe}, k_y c / \omega_{pe})$ plane in log-log scale. The two classes of solution OI-A (“low-frequency,” or nonpropagative) and OI-B (“high-frequency,” or propagative), obtained from the full kinetic dispersion relation (A1)–(A2), are noted A and B, respectively.

related to the OI-B mode is not a trivial task, from a numerical point of view (e.g., the fact that both OI-A and OI-B modes overlap in a region in the wavevector space, makes it difficult to distinguish them). Details of the procedure with which the OI-B branch has been identified, by using the polynomial dispersion relation obtained using an extended fluid description including the full pressure dynamics, so as to “guide” the research of the kinetic roots, can be found in Ref. [5].

In the overlapping region, both OI-A and OI-B modes can be resonantly excited for the same values of k_x and k_y , if the appropriate resonant conditions on the respective phase velocities are met. In general, their propagative character gives them the possibility to resonate and/or nonlinearly couple with higher frequency perturbations. So, in spite of the smaller growth rate of both the non-resonant CFI mode [which has $Re(\omega) = 0$] and of the lower-frequency OI-A modes [which have $Re(\omega) \ll \omega_{pe}$], OI-B modes can play an important role for the emergence of a direct cascade process, which is in turn a preliminary step for the appearance of a developed turbulence.

Appendix B: Further details about the Kuramoto-type synchronization and entropy fluctuations.—The Kuramoto-type description of the Hamiltonian Vlasov system, introduced in the phase synchronization section, allows us to introduce an entropy density $S_{\mathbf{k}} = k_B \ln(1/|f_{\mathbf{k}}(\mathbf{p}, t)|)$ for each Van Kampen mode \mathbf{k} . $S_{\mathbf{k}}$ is equivalent to a Boltzmann entropy, with the quantity $W = 1/|f_{\mathbf{k}}(\mathbf{p}, t)|$ representing the number of configurations (i.e., of Boltzmann’s “complexions”) of a population of oscillators of wave vector included between \mathbf{k} and $\mathbf{k} + d\mathbf{k}$, for a given momentum \mathbf{p} . Entropy is of course conserved in the case of the “kinematic filamentation” associated with the free streaming distribution of a bunch particles (i.e., of an f evolving in absence of forces and collisions): an exact solution of the free advection equation in the

Fourier space, $f_k(v, t) = f_k(v, 0)e^{ikvt}$, yields $S_k(v, t) = k_B \ln [1/|f_k(v, 0)|] = S_k(v, 0)$. In presence of large amplitude, small-scale phase-space fluctuations of f , however, the conservation of Casimir invariants of the Vlasov-Maxwell system is not granted anymore: the conservation of Casimir integrals is indeed formally “measured” in terms of weak convergence, which demands a certain regularity of the solution of the transport equation [18–20]. In the presence of forces in the transport equation, plasma instabilities can make small-scale, large-amplitude fluctuations of f appear (what we called “dynamic filamentation”), which therefore allows macroscopic variations of the entropy, in spite of the Hamiltonian character of the Vlasov-Maxwell system. This is the case of the enhanced filamentation, which we have here identified in a Kuramoto-type description, by linking the formation of filaments in the phase space, i.e., of particle acceleration, to the variation of the L^2 norm or “phasesstrophy flux,” which is known to provide a good proxy for the momentum transfer associated to the fluctuations of the distribution function [53,54]. Combination of filamentation and of coarse graining related to phase mixing allows for an increase of the Shannon entropy S . In the limit of a finite number of Kuramoto-type oscillators φ_i with frequencies ω_i , as they are expressed in the action-angle formalism [cf. phase synchronization section, below Eq. (3)], a Kolmogorow-Sinai entropy production rate $\sigma \equiv dS/dt = k_B Kr \sum_i \sin(\bar{\varphi} - \varphi_i)$ can be shown to fulfill $d^2S/dt^2 = (1/k_B) \sum_i^N (\partial\sigma/\partial\varphi_i)^2 \geq 0$ by formal identification $\varphi_i - \omega_i t \rightarrow \phi_i$ in Eq. (38) of Ref. [75]. In these terms can be interpreted the \mathcal{T}_2 transformation of Fig. 4. On the other hand, as the Kuramoto-type phase synchronization goes on, a decrease of the entropy density S_k , is expected, once the number of independent Van Kampen oscillators is diminished in a globally synchronized state: this agrees with the \mathcal{T}_3 transformation of Fig. 4. Conversely, one can expect good entropy conservation only if the processes of phase synchronization and filamentation lead to mutually canceling entropy fluctuations (transformation \mathcal{T}_1 of Fig. 4, associated to the linear growth of the initial OIs). Quantifying then the amount of entropy which may be produced or reduced (i.e., of information which may be lost or “organized”) in a reversible rather than in an irreversible way during each transformation $\mathcal{T}_1 - \mathcal{T}_3$ is a task which deserves a dedicated study on its own, of both numerical and theoretical character, and it will be discussed elsewhere.

* alain.ghizzo@univ-lorraine.fr

† daniele.del-sarto@univ-lorraine.fr

‡ homam.betar@univ-amu.fr

[1] G. F. Swadling, C. Bruulsema, F. Fiuza, D. P. Higginson, C. M. Huntington, H. S. Park, B. B. Pollock, W. Rozmus,

- H. G. Rinderknecht, J. Katz, A. Birkel, and J. S. Ross, Measurement of Kinetic-Scale Current Filamentation Dynamics and Associated Magnetic Fields in Interpenetrating Plasmas, *Phys. Rev. Lett.* **124**, 215001 (2020).
- [2] D. P. Higginson *et al.*, Laboratory investigation of particle acceleration and magnetic field compression in collisionless colliding fast plasma flows, *Commun. Phys.* **2**, 60 (2019).
- [3] K. I. Nishikawa, P. Hardee, G. Richardson, R. Preece, H. Sol, and G. J. Fishman, Particle acceleration in relativistic jets due to Weibel instability, *Astrophys. J.* **595**, 555 (2003).
- [4] C. M. Huntington, A. G. R. Thomas, C. McGuffey, T. Matsuoka, V. Chvykov, G. Kalintchenko, S. Kneip, Z. Najmudin, C. Palmer, V. Yanovsky, A. Maksimchuk, R. P. Drake, T. Katsouleas, and K. Krushelnick, Current Filamentation Instability in Laser Wakefield Accelerators, *Phys. Rev. Lett.* **106**, 105001 (2011).
- [5] A. Ghizzo, M. Sarrat, and D. Del Sarto, Low- and high-frequency nature of oblique filamentation modes. I. Linear theory, *Phys. Plasmas* **27**, 072103 (2020).
- [6] M. Sarrat, A. Ghizzo, D. Del Sarto, and L. Serrat, Parallel implementation of a relativistic semi-Lagrangian Vlasov-Maxwell solver, *Eur. Phys. J. D* **71**, 271 (2017).
- [7] J. Derouillat, A. Beck, F. Pérez, T. Vinci, M. Chiamello, A. Grassi, M. Flé, G. Bouchard, I. Plotnikov, N. Aunai, J. Dargent, C. Riconda, and M. Grech, SMILEI: A collaborative, open-source, multi-purpose particle-in-cell code for plasma simulation, *Comput. Phys. Commun.* **222**, 351 (2018).
- [8] N. G. Van Kampen, On the theory of stationary waves in plasmas, *Physica* **21**, 949 (1955).
- [9] A. Ghizzo and D. Del Sarto, Low- and high-frequency nature of oblique filamentation modes. II. Vlasov-Maxwell simulations of collisionless heating process, *Phys. Plasmas* **27**, 072104 (2020).
- [10] G. A. Askar'yan, S. V. Bulanov, F. Pegoraro, and A. M. Pukhov, Magnetic interaction of self-focusing channels and fluxes of electromagnetic radiation: Their coalescence, the accumulation of energy and the effect of external magnetic fields on them, *JETP Lett.* **60**, 251 (1994), http://www.jetpletters.ru/ps/1324/article_20333.shtml.
- [11] P. Bertrand, D. Del Sarto, and A. Ghizzo, *The Vlasov Equation I: History and General Properties* (ISTE Ltd, London and Wiley and Sons, New York, 2019), 10.1002/9781119476801.
- [12] B. Kadomtsev and O. Partchevski, *Phénomènes Collectifs dans les Plasmas* (Editions MIR 1979, ISTE—Wiley and Sons, New York, 2019).
- [13] S. H. Strogatz, R. E. Mirollo, and P. C. Matthews, Coupled Nonlinear Oscillators Below the Synchronization Threshold: Relaxation by Generalized Landau Damping, *Phys. Rev. Lett.* **68**, 2730 (1992).
- [14] Z. B. Guo, Y. H. Wang, and S. K. Xu, Phase condensation and evaporation: Another look at wave-particle interactions and Landau damping, *Phys. Rev. E* **101**, 030201(R) (2020).
- [15] S. Xu, Z. B. Guo, and Ö. D. Gürçan, Transition from linear Landau damping to nonlinear Bersnstein-Greene-Kruskal modes via phase synchronization, *Phys. Rev. E* **103**, 023208 (2021).

- [16] A. Ghizzo and D. Del Sarto, The model of particles modes I. A paradigm for phase synchronization in tokamak turbulence, *Phys. Plasmas* **29**, 042506 (2022).
- [17] A. Ghizzo and D. Del Sarto, The model of particles modes II. Transition to a fishbone-like state triggered by global synchronization and energetic particles, *Phys. Plasmas* **29**, 042507 (2022).
- [18] R. J. Diperna and P. L. Lions, Global weak solutions of Vlasov-Maxwell systems, *Commun. Pure Appl. Math.* **42**, 729 (1989).
- [19] G. Rein, Global weak solutions to the relativistic Vlasov-Maxwell system revisited, *Commun. Math. Sci.* **2**, 145 (2004).
- [20] C. Villani, Particle systems and nonlinear Landau damping, *Phys. Plasmas* **21**, 030901 (2014).
- [21] E. S. Weibel, Spontaneous Growing Transverse Waves in a Plasma Due to an Anisotropic Velocity Distribution, *Phys. Rev. Lett.* **2**, 83 (1959).
- [22] B. D. Fried, Mechanism for instability of transverse plasma waves, *Phys. Fluids* **2**, 337 (1959).
- [23] A. Bret, M. C. Firpo, and C. Deutsch, Characterization of the Initial Filamentation of a Relativistic Electron Beam Passing through a Plasma, *Phys. Rev. Lett.* **94**, 115002 (2005).
- [24] A. Bret, L. Gremillet, and D. Bénisti, Exact relativistic kinetic theory of the full unstable spectrum of an electron-beam-plasma system with Maxwell-Jüttner distribution functions, *Phys. Rev. E* **81**, 036402 (2010).
- [25] A. Bret, L. Gremillet, and M. E. Dieckmann, Multidimensional electron beam-plasma instabilities in the relativistic regime, *Phys. Plasmas* **17**, 120501 (2010).
- [26] M. Sarrat, D. Del Sarto, and A. Ghizzo, Fluid description of Weibel-type instabilities via full pressure tensor dynamics, *Europhys. Lett.* **115**, 45001 (2016).
- [27] See Supplemental Material at <http://link.aps.org/supplemental/10.1103/PhysRevLett.131.035101> for more technical details of the Vlasov model and on the role of filamentation (Sec. 1); a summary of the correspondence between the Vlasov and Kuramoto models and thermodynamics aspects associated with entropy production (Sec. 1); a discussion on the complementarity of PIC and semi-Lagrangian numerical schemes (Sec. 2); a summary of the numerical parameters used in all simulations cases A, B, and C (Sec. 2); some further comparison of results obtained with SMILEI and VLEM (Sec. 2); an animation showing the details of the formation of enhanced filamentation in the simulation case B performed with the SMILEI code, and which includes Refs. [28–42].
- [28] M. R. Feix and P. Bertrand, A universal model: The Vlasov equation, *Transp. Theory Stat. Phys.* **34**, 1 (2005).
- [29] C. Mouhot and C. Villani, On Landau damping, *Acta Math.* **207**, 29 (2011).
- [30] V. Zhdankin, Generalized Entropy Production in Collisionless Plasma Flows and Turbulence, *Phys. Rev. X* **12**, 031011 (2022).
- [31] A. C. Kalloniatis, Entropy and stability of phase synchronization of oscillators on networks, *Ann. Phys. (Amsterdam)* **348**, 127 (2014).
- [32] <https://smileipic.github.io/Smilei/>.
- [33] J. M. Dawson, Computer modeling of plasma: Past, present and future, *Phys. Plasmas* **2**, 2189 (1995).
- [34] J. M. Dawson, Particle simulation Plasmas, *Rev. Mod. Phys.* **55**, 403 (1983).
- [35] C. K. Birdsall and A. B. Langdon, *Plasma Physics via Computer Simulation* (Institute of Physics Publishing, Bristol, Philadelphia, 1991), 10.1201/9781315275048.
- [36] P. Bertrand, A. Ghizzo, T. W. Johnston, M. Shoucri, E. Fijalkow, and M. R. Feix, A nonperiodic Euler-Vlasov code for the numerical simulation of laser-plasma beatwave acceleration and Raman scattering, *Phys. Fluids B* **2**, 1028 (1990).
- [37] A. Ghizzo, F. Huot, and P. Bertrand, A non-periodic 2D semi-Lagrangian Vlasov code for laser-plasma interaction on parallel computer, *J. Comput. Phys.* **186**, 47 (2003).
- [38] M. L. Begue, A. Ghizzo, and P. Bertrand, Two-dimensional Vlasov simulation of Raman scattering and plasma beatwave acceleration on parallel computers, *J. Comput. Phys.* **151**, 458 (1999).
- [39] F. Huot, A. Ghizzo, P. Bertrand, E. Sonnendrucker, and O. Coulaud, Instability of the time splitting scheme for the one-dimensional and relativistic Vlasov-Maxwell system, *J. Comput. Phys.* **185**, 512 (2003).
- [40] E. Sonnendrucker, J. Roche, P. Bertrand, and A. Ghizzo, The semi-Lagrangian method for the numerical resolution of the Vlasov equations, *J. Comput. Phys.* **149**, 201 (1998).
- [41] A. J. Klimas, A method for overcoming the velocity space filamentation problem in collisionless plasma model solution, *J. Comput. Phys.* **68**, 202 (1987).
- [42] A. F. Vinas and A. J. Klimas, Flux-balance Vlasov simulation with filamentation filtration, *J. Comput. Phys.* **375**, 983 (2018).
- [43] D. Del Sarto, F. Pegoraro, and F. Califano, Pressure anisotropy and small spatial scales induced by velocity shear, *Phys. Rev. E* **93**, 053203 (2016).
- [44] Y. Yang, W. H. Matthaeus, T. N. Parashar, P. Wu, M. Wan, Y. Shi, S. Chen, V. Roytershteyn, and W. Daughton, Energy transfer channels and turbulence cascade in Vlasov-Maxwell turbulence, *Phys. Rev. E* **95**, 061201(R) (2017).
- [45] P. A. Cassak and M. H. Barbhuiya, Pressure-strain interaction. III. Particle-in-cell simulations of magnetic reconnection, *Phys. Plasmas* **29**, 122308 (2022).
- [46] Y. Kuramoto, *Chemical Oscillations, Waves and Turbulence* (Springer-Verlag, Berlin, 1984).
- [47] J. A. Acebrón, L. L. Bonilla, C. J. Pérez Vicente, F. Ritort, and R. Spigler, The Kuramoto model: A simple paradigm for synchronization phenomena, *Rev. Mod. Phys.* **77**, 137 (2005).
- [48] V. Garcia-Morales, J. Pellicier, and J. A. Manzanares, Thermodynamics based on the principle of least abbreviated action: Entropy production in a network of coupled oscillators, *Ann. Phys. (Amsterdam)* **323**, 1844 (2008).
- [49] A. C. Kalloniatis, Entropy and stability of phase synchronization of oscillators on networks, *Ann. Phys. (Amsterdam)* **348**, 127 (2014).
- [50] A. Nordenfelt, Entropy constraints on convergence in the infinite-N Kuramoto model, *Chaos* **25**, 073109 (2015).
- [51] M. D. Kruskal and C. R. Oberman, On the stability of plasma in static equilibrium, *Phys. Fluids* **1**, 275 (1958).

- [52] P. J. Morrison, The energy of perturbations for Vlasov plasmas, *Phys. Plasmas* **1**, 1447 (1994).
- [53] P. H. Diamond, S. I. Itoh, and K. Itoh, *Modern Plasma Physics, Vol I, Physical kinetics of Turbulent Plasmas* (Cambridge University Press, Cambridge, England, 2010), p. 309.
- [54] A. Ghizzo and D. Del Sarto, Momentum transfer driven by fluctuations in relativistic counter-propagating electron beams, *Plasma Phys. Controlled Fusion* **63**, 055007 (2021).
- [55] F. Califano, N. Attico, F. Pegoraro, G. Bertin, and S. V. Bulanov, Fast Formation of Magnetic Islands in a Plasma in the Presence of Counterstreaming Electrons, *Phys. Rev. Lett.* **86**, 5293 (2001).
- [56] F. Califano, T. Cecchi, and C. Chiuderi, Nonlinear kinetic regime of the Weibel instability in an electron-ion plasma, *Phys. Plasmas* **9**, 451 (2002).
- [57] J. Sakai, S. Saito, H. Mae, D. Farina, M. Lontano, F. Califano, F. Pegoraro, and S. V. Bulanov, Ion acceleration, magnetic field line reconnection, and multiple current filament coalescence of a relativistic electron beam in a plasma, *Phys. Plasmas* **9**, 2959 (2002).
- [58] H. Karimabadi, W. Daughton, and K. B. Quest, Role of electron temperature anisotropy in the onset of magnetic reconnection, *Geophys. Res. Lett.* **31**, L18801 (2004).
- [59] C. Shukla, A. Kumar, A. Das, and B. G. Patel, Merger and reconnection of Weibel separated relativistic electron beam, *Phys. Plasmas* **25**, 022123 (2018).
- [60] R. Pellat, About 'reconnection' in a collisionless plasma, *Space Sci. Rev.* **23**, 359 (1979).
- [61] L. M. Zeleny and A. L. Taktakishvili, Spontaneous magnetic reconnection mechanisms in plasma, *Astrophys. Space Sci.* **134**, 185 (1987).
- [62] H. J. Ziegler and H. Wiechen, Mixing and relaxation in ideal incompressible fluids, *Phys. Scr. T* **74**, 50 (1998).
- [63] D. Grasso, F. Califano, F. Pegoraro, and F. Porcelli, Phase-Mixing and Island Saturation in Hamiltonian Reconnection, *Phys. Rev. Lett.* **86**, 5051 (2001).
- [64] G. Laval, The birth of the research on the magnetic confinement for nuclear fusion, *C.R. Phys.* **20**, 706 (2019).
- [65] P. A. Cassak, M. H. Barbhuiya, H. Liang, and M. R. Argall, Quantifying Energy Conversion in High-Order Phase-Space Density Moments in Plasmas, *Phys. Rev. Lett.* **130**, 085201 (2023).
- [66] H. Wiechen and H. J. Ziegler, Magnetic reconnection: On new aspects of the microscopic cause of localized dissipation, *Phys. Scr. T* **74**, 14 (1998).
- [67] C. Konz, H. Wiechen, and H. Lesch, Shear-flow driven current filamentation: Two-dimensional magnetohydrodynamic-simulations, *Phys. Plasmas* **7**, 5159 (2000).
- [68] J. D. Huba, N. T. Gladd, and K. Papadopoulos, The lower-hybrid-drift instability as a source of anomalous resistivity for magnetic field line reconnection, *Geophys. Res. Lett.* **4**, 125 (1977).
- [69] F. V. Coroniti, Space plasma turbulent dissipation: Reality or myth?, *Space Sci. Rev.* **42**, 399 (1985).
- [70] H. Wiechen, New aspects of plasma sheet dynamics—MHD and kinetic theory, *Ann. Geophys.* **17**, 595 (1999).
- [71] A. Vanthieghem, M. Lemoine, I. Plotnikov, A. Grassi, M. Grech, L. Gremillet, and G. Pelletier, Physics and phenomenology of weakly magnetized, relativistic astrophysical shock jets, *Galaxies* **8**, 33 (2020).
- [72] A. Vanthieghem, M. Lemoine, and L. Gremillet, Origine of intense electron heating in relativistic blast waves, *Astrophys. J. Lett.* **930**, L8 (2022).
- [73] R. Bandyopadhyay, W. H. Matthaeus, T. N. Parashar, Y. Yang, A. Chasapis, B. L. Giles, D. J. Gershman, C. J. Pollock, C. T. Russel, R. J. Strangeway, R. B. Torbert, T. E. Moore, and J. L. Burch, Statistics of Kinetic Dissipation in the Earth's Magnetosheath: MMS Observations, *Phys. Rev. Lett.* **124**, 255101 (2020).
- [74] J. P. Eastwood, M. V. Goldman, T. D. Phan, J. E. Stawarz, P. A. Cassak, J. F. Drake, D. Newman, B. Lavraud, M. A. Shay, R. E. Ergun, J. L. Burch, D. J. Gershman, B. L. Giles, P. A. Lindqvist, R. B. Torbert, R. J. Strangeway, and C. T. Russel, Energy Flux Densities Near the Electron Dissipation Region in Asymmetric Magnetopause Reconnection, *Phys. Rev. Lett.* **125**, 265102 (2020).
- [75] V. Garcia-Morales, J. Pellicer, and J. A. Manzanares, Thermodynamics based on the principle of least abbreviated action: Entropy production in a network of coupled oscillators, *Ann. Phys. (Amsterdam)* **323**, 1844 (2008).